Spectral Decomposition of Missing Transverse Energy at Hadron Colliders

Kyu Jung Bae,[1,*] Tae Hyun Jung,[1,†] and Myeonghun Park[1,2,‡]
[1]Center for Theoretical Physics of the Universe, Institute for Basic Science (IBS), Daejeon 34051, Korea
[2]School of Liberal Arts, Seoul-Tech, Seoul 139-743, Korea

(Received 22 June 2017; revised manuscript received 22 November 2017; published 28 December 2017)

We propose a spectral decomposition to systematically extract information of dark matter at hadron colliders. The differential cross section of events with missing transverse energy ($\not{E}_T$) can be expressed by a linear combination of basis functions. In the case of s-channel mediator models for dark matter particle production, basis functions are identified with the differential cross sections of subprocesses of virtual mediator and visible particle production while the coefficients of basis functions correspond to dark matter invariant mass distribution in the manner of the Källén-Lehmann spectral decomposition. For a given $\not{E}_T$ data set and mediator model, we show that one can differentiate a certain dark matter–mediator interaction from another through spectral decomposition.

DOI: 10.1103/PhysRevLett.119.261801

Introduction.—Cosmological and astrophysical observations have seen strong clues of dark matter (DM) from its gravitational interaction. For its observed thermal relic density, DM particles are believed to have nongravitational interactions with the standard model (SM) particles, for example, weakly interacting massive particles [1,2]. In order to probe such DM particles, many experiments have been conducted [3,4].

Understanding DM production processes at colliders is of great importance for the investigation of DM annihilation in the early Universe due to the time reversal symmetry [5]. To identify interactions between DM and SM particles, many studies have utilized initial state radiation (ISR) with a missing (transverse) energy at linear colliders [6,7] and the Large Hadron Collider (LHC) [8,9].

Here we point out that one of the best ways to analyze DM signals at colliders is to reconstruct DM invariant mass ($m_{\chi\chi}$) distributions. By looking at $m_{\chi\chi}$ distribution, we can extract many properties of dark sector: e.g., masses and spins of DM particles and information about the mediator(s). In the case of a linear collider, we know the initial energy and momentum, so we are able to reconstruct $m_{\chi\chi}$ from the recoil energy, $m_{\chi\chi}^2 = (P_0 - \sum_{\rm vis} P_{\rm vis})^2$, where $P_0 = (E_{\rm CM}, \vec{0})$ is the initial four momentum and $P_{\rm vis}$ are four momenta of outgoing visible particles. In contrast, the $m_{\chi\chi}$ reconstruction is not available at hadron colliders due to the ignorance of initial beam-directional momentum P_z of incoming partons. Alternatively, we can utilize transverse momenta of visible particles to reconstruct a missing transverse energy, $\not{E}_T = |\sum_{\rm vis} \vec{P}^T_{\rm vis}|$, where $\vec{P}^T_{\rm vis}$s are transverse components of three momenta of visible particles. For this reason, previous studies analyzing DM signals at hadron colliders had to rely on the template fitting method simulated by Monte Carlo (MC) tools which maps models to the $\not{E}_T$ distribution. However, this approach is highly model dependent. To cover various DM models, we need to generate corresponding MC simulations for each DM scenario.

In this Letter, we propose a spectral decomposition to extract $m_{\chi\chi}$ distribution at hadron colliders from the $\not{E}_T$ distribution. Spectral decomposition has been used in various fields. One of the most famous examples is Fourier transformation, the decomposition of a function into the linear combination of sinusoidal functions. In a similar way, we define proper basis functions and decompose the $\not{E}_T$ distribution into the linear combination of basis functions. The coefficients correspond to the DM invariant mass distribution. Note that basis functions in the $\not{E}_T$ space have to be linearly independent but not necessarily orthogonal, unlike the Fourier analysis.

Method.—For simplicity and comprehensibility, we concentrate on the s-channel scalar mediator. Our method is applicable to cases of s-channel vector mediators and we summarize with a short proof in the Supplemental Material [10]. We leave the study of the t-channel mediator for future work.

Basis functions used in the spectral decomposition are defined by differential cross sections, the Feynman diagram of which is given in Fig. 1 (right). In Fig. 1, VP denotes associated visible particles, and ϕ is the physical mediator whose mass is M_ϕ. In order to define basis functions, we introduce virtual mediators $\{\phi_i\}$, whose masses are assigned according to the invariant mass of dark matter particles, $m_{\phi_i} = m^{(i)}_{\chi\chi}$ for $i \in \{1, \ldots, N\}$.

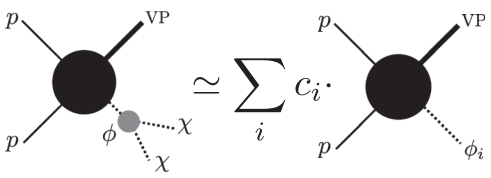

FIG. 1. A schematic diagram of the spectral decomposition of DM production.

With a set of basis functions, the spectral decomposition can be understood by Fig. 1; the differential cross section of the DM production associated with VP [Fig. 1 (left)] is described by the linear combination of differential cross sections of the virtual mediator production [Fig. 1 (right)]. Mathematically, it is expressed as

$$\frac{d\sigma^{\rm exp}(X)}{dX} \simeq \sum_{i=1}^{N} c_i \underbrace{\left(\frac{1}{\mathcal{N}_i}\frac{d\sigma_{\phi_i}(X)}{dX}\right)}_{=\text{basis functions}}, \tag{1}$$

where X is a collider observable, e.g., $\not{E}_T$ or the transverse momentum of the ISR jet. $\mathcal{N}_i$s are normalization factors, $d\sigma^{\rm exp}/dX$ is the differential cross section of physical process [$pp \to \text{VP} + \text{DM}$: Fig. 1 (left)] and $d\sigma_{\phi_i}/dX$ is the differential cross section of the virtual mediator production [$pp \to \text{VP} + \phi_i$: Fig. 1 (right)]. The normalization factor $\mathcal{N}_i$ is given by

$$\mathcal{N}_i = \int_{X_{\rm min}}^{X_{\rm max}} dX \frac{d\sigma_{\phi_i}(X)}{dX}, \tag{2}$$

where $[X_{\rm min}, X_{\rm max}]$ is a range of X determined by cuts. For applying our method to data analyses, we discretize $[X_{\rm min}, X_{\rm max}]$ into $\{X_{\rm bin}\}$.

We regard the lhs of Eq. (1) as experimental signal data after background subtraction and the rhs of Eq. (1) as the model hypothesis. Here, the c_is in Eq. (1) are fitting parameters. One can obtain $\{c_i\}$ from the standard χ^2 fitting, which minimizes

$$\chi^2 = \sum_{X_{\rm bin}} \frac{(\text{Ex}(X_{\rm bin}) - \text{SM}(X_{\rm bin}) - \sum_{i=1}^{N} c_i F_i(X_{\rm bin}))^2}{\text{Ex}(X_{\rm bin})}, \tag{3}$$

where $\text{Ex}(X_{\rm bin})$ is the experimental number of events in $X \in X_{\rm bin}$, $\text{SM}(X_{\rm bin})$ is obtained by the SM background calculation, and $F_i(X_{\rm bin})$ corresponds to basis functions given by

$$F_i(X_{\rm bin}) = \frac{L}{\mathcal{N}_i} \int_{X \in X_{\rm bin}} dX \frac{d\sigma_{\phi_i}(X)}{dX}, \tag{4}$$

with a given integrated luminosity L. In order to obtain a unique solution from χ^2 fitting, basis functions should be linearly independent.

If X is $\not{E}_T$ determined by ISR, the differential distribution of X depends on a hard scale of a parton distribution function (PDF). When $\not{E}_T$ is much smaller than m_{ϕ_i}, the hard scale is mostly determined by m_{ϕ_i}. In the opposite case where $\not{E}_T$ is larger than m_{ϕ_i}, the hard scale is proportional to $\not{E}_T$. In other words, m_{ϕ_i} is the characteristic scale which determines the shape of corresponding basis function. In this regard, basis functions are linearly independent.

In our analyses, we have numerically confirmed linear independence by examining

$$\min_{d_j}\left[\sum_{X_{\rm bin}}\left(N_s F_i(X_{\rm bin}) - \sum_{j\neq i} d_j F_j(X_{\rm bin})\right)^2 / \text{Ex}(X_{\rm bin})\right] \geq \epsilon, \tag{5}$$

for all i and given total number of signal events N_s where $\min_{d_j}$ is minimization for parameters d_j. A positive parameter ϵ is introduced to take into account statistical fluctuation. In our analyses with seven basis functions and $S/B = 1/100$, ϵ is 7.01 with 68% confidence level. A general discussion on the validity of this method can be found in Ref. [12].

In order to explicitly show the procedure, let us consider the DM model whose Lagrangian is written as

$$\mathcal{L} = \mathcal{L}_{\rm SM} + \underbrace{\mathcal{L}_{\rm med-SM} + \mathcal{L}_{\rm med}}_{\to\text{basis functions}} + \underbrace{\mathcal{L}_{\rm med-DM} + \mathcal{L}_{\rm DM}}_{\to\text{spectral density}}, \tag{6}$$

where $\mathcal{L}_{\rm SM}$ is the SM Lagrangian, $\mathcal{L}_{\rm med-SM}$ ($\mathcal{L}_{\rm med-DM}$) is the interaction Lagrangian between the mediator and SM particles (DM particles). $\mathcal{L}_{\rm med}$ ($\mathcal{L}_{\rm DM}$) is the kinetic term for the mediator (DM particles) including its mass. $\mathcal{L}_{\rm med-SM} + \mathcal{L}_{\rm med}$ affects only basis functions while $\mathcal{L}_{\rm med-DM} + \mathcal{L}_{\rm DM}$ governs c_i. The procedure of our method is described by following steps: (1) Fix $\mathcal{L}_{\rm med-SM} + \mathcal{L}_{\rm med}$ and calculate basis functions. (2) Obtain $\{c_i\}$ by applying Eq. (3) to the signal data. (3) Find the proper $\mathcal{L}_{\rm med-DM} + \mathcal{L}_{\rm DM}$ that matches with obtained $\{c_i\}$. It is worth noting that one needs to specify $\mathcal{L}_{\rm med-SM}$ in order to construct basis functions. For example, basis functions where the mediator is produced through gluon-gluon fusion is different from those where it is produced through quark and antiquark annihilation. However, CP charge of a mediator does not affect basis functions when the mediator is in the s channel. We have numerically confirmed that $\phi G_{\mu\nu} G^{\mu\nu}$ and $\phi G_{\mu\nu} \tilde{G}^{\mu\nu}$ amount to the same basis functions. (For other interactions, it can be inferred from Ref. [9].) The mediator models (i.e., $\mathcal{L}_{\rm med-DM}$) can be inferred by other collider variables such as an angular correlation between jets in the $jj + \not{E}_T$ channel [13]. It is also possible to concentrate on the test of mediator itself by using a visible decay mode and checking its consistency [14].

Spectral density.—The physical meaning of c_i is the DM invariant mass ($m_{\chi\chi}$) distribution,

$$c_i \simeq \frac{d\sigma^{\rm exp}(m_{\chi\chi}^{(i)})}{dm_{\chi\chi}} \Delta m_{\chi\chi}^{(i)}, \tag{7}$$

where $\Delta m_{\chi\chi}^{(i)} = (m_{\chi\chi}^{(i+1)} - m_{\chi\chi}^{(i-1)})/2$. c_i is related to the Källén-Lehmann spectral density $\rho_{\phi\to\chi\chi}(m_{\chi\chi}^{(i)}, M_\phi)$ [15] by

$$c_i = 2 m_{\chi\chi}^{(i)} \Delta m_{\chi\chi}^{(i)} \mathcal{N}_i \rho_{\phi\to\chi\chi}(m_{\chi\chi}^{(i)}, M_\phi). \tag{8}$$

The spectral density $\rho_{\phi\to\chi\chi}(m_{\chi\chi}^{(i)}, M_\phi)$ is given by

$$\rho_{\phi\to\chi\chi}(m_{\chi\chi}^{(i)}, M_\phi) = \frac{1}{\pi} |G_\phi(m_{\chi\chi}^{(i)}, M_\phi)|^2 m_{\chi\chi}^{(i)} \Gamma_{\phi_i\to\chi\chi}(m_{\chi\chi}^{(i)}), \tag{9}$$

where $G_\phi(m_{\chi\chi}^{(i)}, M_\phi)$ is the propagator of ϕ with energy transfer $m_{\chi\chi}^{(i)}$ and on-shell mass M_ϕ, and $\Gamma_{\phi_i\to\chi\chi}(m_{\chi\chi})$ is the decay rate of process $\phi_i \to \chi\chi$ with mass $m_{\phi_i} = m_{\chi\chi}$. $\rho_{\phi\to\chi\chi}(m_{\chi\chi}^{(i)}, M_\phi)$ does not depend on collider observables, X (e.g., p_T, rapidity, or $\not{E}_T$, etc.), or cut variables. In addition, it is independent of channels (e.g., monojet, mono-Z, etc.) and collider energy. This feature guarantees that the spectral decomposition is valid up to detector level. Mathematical proofs are given in the Supplemental Material [10] and its numerical validation is given in the next section.

Although basis functions depend on mediator models, the spectral decomposition method make analyses less model dependent. Once we specify $\mathcal{L}_{\text{med-SM}} + \mathcal{L}_{\text{med}}$ (step 1), we can obtain spectral density from the signal data (step 2) and infer $\mathcal{L}_{\text{med-DM}} + \mathcal{L}_{\text{DM}}$ through physical insights (step 3).

Here, we discuss some possible cases for the connection between spectral densities and the DM interactions in $\mathcal{L}_{\text{med-DM}} + \mathcal{L}_{\text{DM}}$. When a mediator ϕ is heavier than the DM threshold ($M_\phi > 2m_\chi$), $\rho_{\phi\to\chi\chi}$ will be described by the Breit-Wigner distribution. In the case of $M_\phi < 2m_\chi$, $\rho_{\phi\to\chi\chi}$ will be proportional to the power of DM's velocity v_χ, $\rho_{\phi\to\chi\chi} \propto v_\chi^{2J_0+1}$. If $m_\chi < M_\phi < 2m_\chi$ and the dominant annihilation can be $\chi\chi \to$ SM particles through the mediator (for $m_\chi > m_\phi$ case, the dominant process can be $\chi\chi \to \phi\phi$), it may be possible to infer the velocity dependence of DM annihilation process at the thermal freeze-out due to the time reversal symmetry [6],

$$\langle \sigma_{\text{ann}} v_\chi \rangle \equiv \sigma_0 v_\chi^{2J_0} + \mathcal{O}(v_\chi^{2J_0+2}), \tag{10}$$

where it corresponds to the s-wave (p-wave) process if $J_0 = 0(1)$. Some nontrivial spectral densities can be obtained when nonrenormalizable operators [8] or resonance spectrum ($M_\phi \simeq 2m_\chi$) [16] are considered.

Compared to previous studies relying on Monte Carlo simulations, the spectral decomposition becomes more powerful when the dark sector is complicated. For example, if there exist several DM species (heavier than M_ϕ), $m_{\chi\chi}$ distribution from the spectral decomposition has multi-threshold behavior. At each threshold, we can count the power of v_χ in order to identify the interaction. For another example, let us consider the production of two mediator particles: one is on shell ($M_{\phi_1} > 2m_\chi$) and the other is off shell ($M_{\phi_2} < 2m_\chi$). Our procedure will recover the Breit-Wigner resonance of the $\phi_1 \to \chi\chi$ process, standing on the middle of continuum distribution from $\phi_2 \to \chi\chi$. Such a situation can be realized in various Higgs portal models, where both Higgs boson and singlet scalar produce DM particles through mixing. In addition, the spectral decomposition can be used to verify whether or not DM particles form a bound state. A bound-state resonance will be located slightly below the DM threshold at the $m_{\chi\chi}$ distribution. The theoretical prediction is obtained by solving the nonrelativistic Schrödinger equation [17], and thus we may able to see the trace of Sommerfeld enhancement in the dark matter annihilation process [18].

LHC example.—In order to show the detail, we provide a specific example where we set the center-of-mass energy to be 14 TeV and the integrated luminosity to be 3 ab^{-1}.

Step 1: Our toy model includes a real scalar mediator ϕ which interacts with SM through the dimension-5 operator,$\phi G^{\mu\nu} G_{\mu\nu}$. We consider the $X = \not{E}_T$ distribution of monojet process ($pp \to j\chi\chi$). Once we fix $\mathcal{L}_{\text{med-SM}} + \mathcal{L}_{\text{med}}$, we can calculate basis functions [i.e., the differential cross section of ($pp \to j\phi_i$)] with a given set of $\{m_{\chi\chi}^{(i)}\}$. In this example, we set $\{m_{\chi\chi}^{(i)}\} = \{10, 200, 400, 700, 1100, 2000, 5000\}$ in GeV units. We take a larger gap between $m_{\chi\chi}^{(i)}$ s at higher $m_{\chi\chi}^{(i)}$ so that the basis functions are distinguishable in $\not{E}_T$ space. For numerical analyses, a number of tools are used: FeynRules2.0/MadGraph_aMC@NLO [19] for parton-level event generation, Pythia 8.1 [20] for parton showering and hadronization, and Delphes3 [21]/FastJet3 [22] for detector-level event reconstruction with ATLAS detector Delphes card. Jets are reconstructed by an anti-k_T algorithm with jet radius parameter 0.4. We select events with $\not{E}_T > 200$ GeV and at least one jet having $p_T^j > 100$ GeV and $|\eta^j| < 2.5$. We choose $\not{E}_T$ bin size to be 10% of $\not{E}_T$, which corresponds to the p_T resolution of the jet at the LHC [23], and the range of $\not{E}_T$ is taken from 200 GeV to 2 TeV.

Step 2: We decompose signal distributions into basis functions according to Eq. (1) with $X = \not{E}_T$. We generate signal distributions from pseudoexperiments (PEs). We choose scalar dark matter (trilinear interaction with the mediator: s-wave) and fermionic dark matter (Yukawa interaction with the mediator: p-wave) for signal distributions. A DM mass is set to be $m_\chi = 200$ GeV, so the threshold is at $2m_\chi = 400$ GeV. In Fig. 2, their $\not{E}_T$ distributions are shown as black dotted lines on the top of each plot.

By following the fitting procedure explained in previous sections, we decompose signal distributions into basis functions. In Fig. 2, it is illustrated that basis functions (shaded by different colors) are piled into the overall distribution (black dotted line). The area of each basis function in Fig. 2 is equal to a normalized coefficient,

$$\hat{c}_i = c_i / \sum c_i, \tag{11}$$

which corresponds to DM invariant mass distribution. Different colors indicate different $m_{\chi\chi}^{(i)}$s, whose corresponding numbers are shown in the bar on the right-hand side. By comparing the areas of two panels in Fig. 2, we can see that the s-wave process (left) tends to be more distributed around the DM threshold ($m_{\chi\chi} = 400$ GeV) than the p-wave process (right).

Step 3: Coefficients $\{\hat{c}_i\}$ show the DM invariant mass distribution from which we can infer the interaction

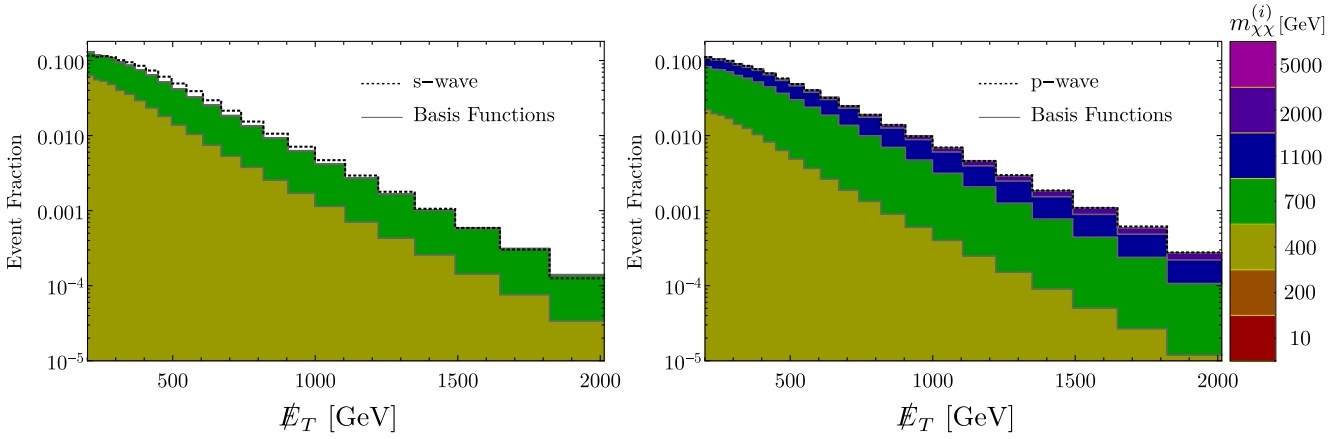

FIG. 2. Missing transverse energy ($\not{E}_T$) distribution of monojet process in toy model. Black dotted lines correspond to the signal distributions of s-wave (left) and p-wave (right) processes. Dark matter mass is set to be 200 GeV. Signal distributions are decomposed into basis functions (colored), whose different colors represent the value of $m_{\chi\chi}^{(i)}$, as in the bar on the right.

between the mediator and DM particles. In Fig. 3, we show four cases of the 200-GeV DM production in $m_{\chi\chi}$: invisible decay of the on-shell mediator (red), s-wave process through the off-shell mediator (green), p-wave through the off-shell mediator (blue) and s-wave process through the off-shell mediator with a DM bound state near threshold (dark green dashed). While the true values of $\hat{c}_i$s are shown in the left panel, $\hat{c}_i$s obtained by our method are shown in the middle (right) panel for signal-to-background ratio $S/B = 1/100$ $(1/250)$. On-shell production of the mediator (red) causes only one bin to be nonzero among the $m_{\chi\chi}^{(i)}$s due to the Breit-Wigner resonance ($m_{\chi\chi} = M_\phi = 700$ GeV). For off-shell cases, coefficients are nonzero in a broad range of $m_{\chi\chi}^{(i)}$s, and the first nonzero bin corresponds to the threshold, $2m_\chi = 400$ GeV. In the case of the s-wave process (green), events are more distributed near the threshold than those in the case of the p-wave process (blue) because of v_χ dependence. If there exists a bound-state resonance (dark green dashed) it makes a larger value in the first nonzero bin. [Here, the bound-state resonance cross section is set to be 15% of the total cross section. Such a case corresponds to $g_{\rm DM}^2/(4\pi) \simeq 0.35$ (where $g_{\rm DM}$ is gauge coupling constant in the dark sector) if the DM particle is in the $\mathrm{SU}(3)_{\rm DM}$ fundamental representation.] In the middle and right panels, statistical errors are denoted by shaded bands (except for bound-state case) and their discrimination power can be estimated. While lines are separated enough to be distinguished for $S/B = 1/100$, there are relatively large overlap in error bands for $S/B = 1/250$. Significances for $S/B = 1/250$ are summarized in Table I.

We estimate errors in fitting c_is by the following procedure. We take the SM background of the $pp \to j + Z(Z \to \nu\bar{\nu})$ parton-level process. A more precise SM estimation can be found in Ref. [24], which also includes $pp \to j + W(W \to l\nu)$ and other processes. To make the expected number of events consistent with Ref. [24], we multiply the energy-dependent K-factor $\mathrm{Max}(1, -\not{E}_T/(400\ \mathrm{GeV}) + 2.6)$. The total number of

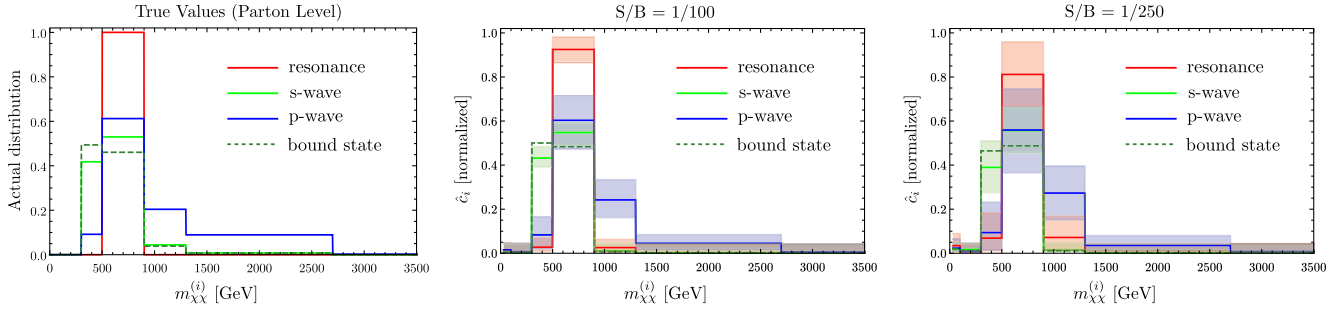

FIG. 3. DM invariant mass ($m_{\chi\chi}$) distribution for DM mass $m_\chi = 200$ GeV, center of mass energy 14 TeV and integrated luminosity $L = 3$ ab^{-1}. We consider four cases: DM particles are produced in resonance decay of the ϕ at 700 GeV (red), in the continuum in the s-wave (green), in the continuum in the p-wave (blue) and in the continuum in the s-wave with bound state near threshold. For the resonance case, $M_\phi = 700$ GeV $> 2m_\chi$ while for other cases, $M_\phi = 30$ GeV. Their true distributions are given in the left panel. In right two panels, $\{\hat{c}_i\}$ obtained by our method are plotted with signal to background ratio $S/B = 1/100$ (middle) and $1/100$ (right).

TABLE I. Expected significance when the signal distribution given in the first column is fitted by hypothesis given in the first row. Signal number of events is fixed by $S/B = 1/250$ with 3 ab^{-1} at 14 TeV.

	Hypothesis			
Signal	Resonance	s-wave	p-wave	Bound state
Resonance		1.62σ	2.22σ	2.15σ
s-wave	4.30σ		4.20σ	0.943σ
p-wave	1.68σ	2.21σ		2.90σ
Bound state	4.48σ	1.33σ	4.45σ	

signal events is fixed by setting $S/B = 1/250$ and $1/100$. For each $\not{E}_T$ bin, we generate 10^4 of pseudoexperiments by a Poissonian random number generator. Then the fitting procedure is repeated to obtain 10^4 different sets of $\{\hat{c}_i^{(\mathrm{PE})}\}$ for each PE. From them, we obtain the probability density distribution of $\{\hat{c}_i\}$ and estimate the expected value of $\{\hat{c}_i\}$ (solid lines) and expected 68% errors (shaded bands).

From this example, we notice that a large number of signal events are required to identify the dark sector. In Fig. 3, the corresponding values of $S/\sqrt{B}$ are 8 (middle) and 3 (right) for 30 fb^{-1} at 13 TeV, which are almost excluded at current LHC searches. Nevertheless, even for the $S/B = 1/250$ benchmark point, some cases in Fig. 3 are distinguishable, and we summarize the corresponding significance in Table I.

The resolution of $m_{\chi\chi}$ (i.e., how small bins can be) can be regarded as the distinguishability of basis functions [i.e., how large ϵ in Eq. (5) is]. While the distinguishability is mostly affected by the statistical fluctuation in our analyses, a real analysis must take into account systematic uncertainties in the calculation of basis functions. In order to precisely estimate systematic uncertainties, full detector simulations with the best tools are required.

Conclusion and discussion.—The spectral decomposition allows us to extract DM invariant mass distribution even at hadron colliders. When DM particles are produced via s-channel mediators, basis functions of the spectral decomposition do not depend on DM properties, while coefficients $\{c_i\}$ (or $\rho_{\chi\to\chi\chi}$) contain detailed information of dark matter particles.

One of the most challenging issues in our approach is the requirement of a large number of signal events to identify the dark sector at hadron colliders. Until now, the LHC has no signal excess of DM in all the mono-X channels: monojet [24], monophoton [25], mono-Z [26], and mono-Higgs [27]. The integrated luminosity is, now, about 30 fb^{-1}. This means that if we set $S/\sqrt{B} < 2$ at $L = 30$ fb^{-1}, then it will become, at most, $S/\sqrt{B} < 20$ at the end of projected high-luminosity run of $L = 3$ ab^{-1}. Nevertheless, it can be resolved if we combine signal data of various channels together with collider observables other than $\not{E}_T$. In addition, in the next-generation collider (e.g., a 100-TeV proton-proton collider), better S/B can be achieved in DM signals, so the spectral decomposition is useful to understand the dark sector.

This work is supported by the Institute for Basic Science under Project No. IBS-R018-D1.

*kyujungbae@ibs.re.kr
†thjung0720@ibs.re.kr
‡parc.seoultech@seoultech.ac.kr

[1] B. W. Lee and S. Weinberg, Phys. Rev. Lett. **39**, 165 (1977).
[2] G. Jungman, M. Kamionkowski, and K. Griest, Phys. Rep. **267**, 195 (1996); G. Bertone, D. Hooper, and J. Silk, Phys. Rep. **405**, 279 (2005).
[3] A. Tan *et al.* (PandaX-II Collaboration), Phys. Rev. Lett. **117**, 121303 (2016); D. S. Akerib *et al.* (LUX Collaboration), Phys. Rev. Lett. **118**, 021303 (2017); C. Amole *et al.* (PICO Collaboration), Phys. Rev. Lett. **118**, 251301 (2017).
[4] M. L. Ahnen *et al.* (MAGIC and Fermi-LAT Collaborations), J. Cosmol. Astropart. Phys. 02 (2016) 039.
[5] W. Frazer, *Elementary Particles* (Prentice-Hall, Englewood Cliffs, NJ, 1966).
[6] A. Birkedal, K. Matchev, and M. Perelstein, Phys. Rev. D **70**, 077701 (2004); J. L. Feng, S. Su, and F. Takayama, Phys. Rev. Lett. **96**, 151802 (2006); P. Konar, K. Kong, K. T. Matchev, and M. Perelstein, New J. Phys. **11**, 105004 (2009).
[7] C. Bartels, O. Kittel, U. Langenfeld, and J. List, arXiv:1202.6516; S. Y. Choi, T. Han, J. Kalinowski, K. Rolbiecki, and X. Wang, Phys. Rev. D **92**, 095006 (2015); T. Kamon, P. Ko, and J. Li, Eur. Phys. J. C **77**, 652 (2017).
[8] D. Barducci, A. Bharucha, N. Desai, M. Frigerio, B. Fuks, A. Goudelis, S. Kulkarni, G. Polesello, and D. Sengupta, J. High Energy Phys. 01 (2017) 078.
[9] A. Belyaev, L. Panizzi, A. Pukhov, and M. Thomas, J. High Energy Phys. 04 (2017) 110.
[10] See Supplemental Material at http://link.aps.org/supplemental/10.1103/PhysRevLett.119.261801 for some proofs, which includes Ref. [11].
[11] C. F. Uhlemann and N. Kauer, Nucl. Phys. **B814**, 195 (2009).
[12] T. H. Jung and M. Park, Extracting Dark Matter Information at Hadron Colliders by Spectral Decomposition Method (to be published).
[13] M. R. Buckley, B. Heinemann, W. Klemm, and H. Murayama, Phys. Rev. D **77**, 113017 (2008); K. Hagiwara, Q. Li, and K. Mawatari, J. High Energy Phys. 07 (2009) 101; M. R. Buckley and M. J. Ramsey-Musolf, J. High Energy Phys. 09 (2011) 094.
[14] ATLAS Collaboration, Summary Plots from the ATLAS Exotic Physics Group (2017).CMS Collaboration, Dark Matter Summary Plots from CMS for LHCP 2017.
[15] M. E. Peskin and D. V. Schroeder, *An Introduction to Quantum Field Theory* (Addison-Wesley, Reading, MA, 1995).
[16] D. Chway, T. H. Jung, and H. D. Kim, J. Korean Phys. Soc. **69**, 16 (2016).

[17] M. J. Strassler and M. E. Peskin, Phys. Rev. D **43**, 1500 (1991).
[18] A. Sommerfeld, Ann. Phys. (Berlin) **403**, 257 (1931); J. Hisano, S. Matsumoto, M. M. Nojiri, and O. Saito, Phys. Rev. D **71**, 063528 (2005); N. Arkani-Hamed, D. P. Finkbeiner, T. R. Slatyer, and N. Weiner, Phys. Rev. D **79**, 015014 (2009).
[19] A. Alloul, N. D. Christensen, C. Degrande, C. Duhr, and B. Fuks, Comput. Phys. Commun. **185**, 2250 (2014); J. Alwall, R. Frederix, S. Frixione, V. Hirschi, F. Maltoni, O. Mattelaer, H.-S. Shao, T. Stelzer, P. Torrielli, and M. Zaro, J. High Energy Phys. 07 (2014) 079.
[20] T. Sjostrand, S. Mrenna, and P. Z. Skands, Comput. Phys. Commun. **178**, 852 (2008).
[21] J. de Favereau, C. Delaere, P. Demin, A. Giammanco, V. Lemaître, A. Mertens, and M. Selvaggi (DELPHES 3 Collaboration), J. High Energy Phys. 02 (2014) 057.
[22] M. Cacciari and G. P. Salam, Phys. Lett. B **641**, 57 (2006); M. Cacciari, G. P. Salam, and G. Soyez, Eur. Phys. J. C **72**, 1896 (2012).
[23] V. Khachatryan *et al.* (CMS Collaboration), J. Instrum. **12**, P02014 (2017).
[24] M. Aaboud *et al.* (ATLAS Collaboration), arXiv: 1711.03301; A. M. Sirunyan *et al.* (CMS Collaboration), arXiv:1712.02345.
[25] M. Aaboud *et al.* (ATLAS Collaboration), Eur. Phys. J. C **77**, 393 (2017); A. M. Sirunyan *et al.* (CMS Collaboration), J. High Energy Phys. 10 (2017) 073.
[26] M. Aaboud *et al.* (ATLAS Collaboration), Phys. Lett. B **776**, 318 (2017); A. M. Sirunyan *et al.* (CMS Collaboration), arXiv:1711.00431.
[27] M. Aaboud *et al.* (ATLAS Collaboration), Phys. Rev. Lett. **119**, 181804 (2017); CMS Collaboration, Report No. CMS-PAS-EXO-16-054, 2017.